Chronology of the late Lower and Middle Palaeolithic at Tabun Cave (Mount Carmel, Israel) with insights into diagenesis and dose rate variation using post-IR IRSL (pIRIR290) dating and infrared spectroscopy

Maïlys Richard, Norbert Mercier, Mina Weinstein-Evron, Lior Weissbrod, Ron Shimelmitz

Chronology of the late Lower and Middle Palaeolithic at Tabun Cave (Mount Carmel, Israel) with insights into diagenesis and dose rate variation using post-IR IRSL ($pIRIR_{290}$) dating and infrared spectroscopy

Richard M.[1,2,3]*, Mercier N.[1], Weinstein-Evron M.[4], Weissbrod L.[5], Shimelmitz R.[4]

[1]Archéosciences Bordeaux, UMR 6034 CNRS-Université Bordeaux Montaigne, 33607 Pessac, France

[2]Scientific Archaeology Unit, Weizmann Institute of Science, 7610001 Rehovot, Israel

[3]Department of Early Prehistory and Quaternary Ecology, University of Tübingen, Tübingen, Germany

[4] Zinman Institute of Archaeology, School of Archaeology and Maritime Cultures, University of Haifa, 3103301, Haifa, Israel

[5]Israel Antiquities Authority, POB 586, Jerusalem, 9100402, Israel.

*corresponding author: mailys.richard@u-bordeaux-montaigne.fr

Abstract

Tabun Cave, located on the slopes of Mount Carmel (Israel), constitutes one of the key Levantine Palaeolithic sites because of its exceptionally long sequence (ca. 25 meters) that has yielded a suite of lithic industries spanning the Lower and Middle Palaeolithic periods. This site is also known to have produced human remains found in the Middle Palaeolithic layers: a Neanderthal female skeleton (C1), and a mandible (C2) commonly classified as *Homo sapiens* but whose attribution is still debated.

Determining the chronology of Levantine Palaeolithic caves has often been limited by severe diagenetic processes, affecting the accuracy of age results obtained using trapped-charge dating methods. Characterising the mineralogical composition of the sediments in such conditions is an important step that was done in this study using Fourier transform infrared (FTIR) spectroscopy. We show that most of our sediment samples underwent diagenesis from the decomposition of guano, ash or bones, based on the presence of authigenic phosphates,

which may impact the dose rate. Considering this information, we report here age results obtained using post-infrared infrared stimulated luminescence ($pIRIR_{290}$) of polymineral fine grains for Tabun Cave.

Our $pIRIR_{290}$ ages are in overall agreement with thermoluminescence (TL) dating results obtained previously on burnt flints, reinforcing the antiquity of key transitions in the Middle Pleistocene record from Tabun Cave. The ages suggest that the Lower to Middle Palaeolithic transition at Tabun, possibly coinciding with the arrival of *Homo sapiens* in the Levant, may be constrained between 265 ± 26 ka (late Lower Palaeolithic, Bed 72, Unit X) and 288 ± 29 ka (early Middle Palaeolithic, Beds 63-64, Unit IX), while the age of the base of the overlying mid-Middle Palaeolithic Layer C (Unit I; Beds 22-19) ranges between 204 ± 18 ka and 192 ± 14 ka. Consequently, the Tabun C2 mandible discovered at the base of Layer C may prove to be among the oldest *Homo sapiens* fossils found outside Africa.

Keywords: $pIRIR_{290}$, FTIR spectroscopy, diagenesis, Palaeolithic, Levant

1. Introduction

The long sequence of Tabun Cave has yielded Lower Palaeolithic (LP) occupations with Acheulean and Acheulo-Yabrudian lithic industries, and Middle Palaeolithic (MP) occupations, with Mousterian industries (Garrod and Bate, 1937; Jelinek et al., 1973) (Fig. 1). It remains debated whether the transition from the LP to the MP in the Levant involved a continuity of lithic traditions or the introduction of new populations (Shimelmitz et al., 2016; Meignen and Bar-Yosef, 2020; Zaidner and Weinstein-Evron, 2020; Shimelmitz et al., 2021). A stratigraphical unit directly underlying the MP deposits was defined by Jelinek (1982) (Unit X) as transitional between the LP and MP, although this attribution has been the subject of debate. The same unit was argued to have been form as a mixture of LP and MP material (Bar-Yosef, 1994). However, a recent investigation of Bed 72, at the bottom of Unit X, shows it is part of the Acheulo-Yabrudian, representing the very end of the LP (Shimelmitz et al., 2021). Accordingly, obtaining precise ages for constraining the very end of the LP and the beginning of the MP at Tabun is of great importance. The timing of this transition in the Levant has been broadly bracketed to 270–200 ka based on age estimates derived from the youngest ages of Acheulo-Yabrudian layers and the earliest ages of early MP layers at Tabun, Qesem and Misliya caves (Fig. 1a, Mercier and Valladas, 2003; Gopher et al., 2010; Mercier et al., 2013; Valladas et al., 2013).

The division of the MP period in the Levant is also debated. Until the end of the 20th century, it was commonly divided into three chrono-cultural phases based on the lithic industries of Tabun Layers D, C, and B (Copeland, 1975), corresponding to the commonly used designations early, middle, and late MP, respectively. The pace of change from one phase to another in this sequence and the extent of similarities in lithic technology across Levantine sites from either one of the phases remains debated as well (e.g., Shea, 2014; Oron et al., 2024). Within this division, the end of the early MP is not well defined, with some researchers placing it as late as ca. 130–140 ka (e.g., Shea, 2014; Zaidner et al., 2021), while others propose it to be around 160 ka (e.g., Valladas et al., 2013; Goder-Goldberger and Bar-Matthews, 2019; Wojtczak and Malinsky-Buller, 2022). The available ages from Tabun Cave reinforce the latter timeline with mean thermoluminesence (TL) ages of 196 ± 21 ka for Layer D (Beds 30 and 32 of Unit II) and 165 ± 16 ka for Layer C (Beds 20 and 21 of Unit I; Mercier and Valladas, 2003).

The different ideas concerning the beginning of the mid-MP in Tabun, with its characteristic technology and connection with the Tabun C2 hominin mandible, has introduced much uncertainty into discussions (Hovers, 2009; Groucutt et al., 2019; Zaidner et al., 2021). Some of the sites ascribed to this cultural and lithic technological phase have provided ages in Marine Isotopic Stage (MIS) 5 (Grün et al., 2005; Hovers, 2009; Zaidner et al., 2021; Barzilai et al., 2022). However, this is in disagreement with the earlier ages from Tabun Layer C that appear to extend the range back into mid MIS 6 (Mercier and Valladas, 2003) and biostratigraphic considerations drawn from the microfaunal assemblages (Weissbrod and Weinstein-Evron, 2022). Thus, new dating is critical to re-evaluate these discrepancies.

Establishing a robust chronological framework for Tabun Cave remains essential to refining the timing of early modern human dispersals, understanding their adaptation to climate change, and examining the possibility of contemporaneity between different human biological groups in the Levant. Previous chronological determinations from Tabun yielded ages which were found to be much older than those of depositional units with similar lithic industries at other regional sites, causing considerable uncertainty in efforts to reconstruct a robust evolutionary sequence for the region. Parts of the Tabun sequence were dated using electron spin resonance (ESR) and ESR combined with U-series (ESR/U-series) of tooth enamel (Grün and Stringer, 2000; Rink et al., 2004) and TL of burnt flints (Mercier et al., 1995b; Mercier et al., 2000; Mercier and Valladas, 2003). The TL results suggest that the sequence between Units XIV and I ranges from ca. 415 ka (bottom of Bed 90, Unit XIV, Mercier et al., 2000) to ca. 165 ka (mean age for the bottom of layer C, Unit I, Mercier and Valladas, 2003). Combined ESR/U-series dating from another part of the cave, associated with the early Acheulo-Yabrudian, has

given an age of ca. 387 ka for this industry (Rink et al., 2004). For the upper part of this sequence, the ESR/U-series age of 135 +60/-30 ka (Grün and Stringer, 2000) is broadly in agreement with the mean TL age of 165 ± 16 ka (Mercier and Valladas, 2003).

This review of the existing chronological data shows that it is essential to bear in mind that trapped-charge dating results from Tabun may have been impacted by diagenetic processes affecting both the dated sample and its depositional environment (Weiner, 2010). This is highlighted in several studies about diagenesis in caves in the Levant (e.g., Weiner et al., 1993; Weiner et al., 2002) and elsewhere (e.g., Karkanas et al., 2000, Han et al., 2010), demonstrating the often severe alterations that archaeological materials and mineralogical assemblages have undergone over time due to geochemical processes. For instance, in Hayonim Cave (Figure 1a), spatial variation in the dose rates (measured with in-situ dosimeters) was observed and correlated with the distribution of authigenic minerals formed on site as a result of diagenesis (Weiner et al., 2002). Mercier et al. (2007) further identified distribution of mineral assemblages in the sections where dosimetry was conducted in relation to the location of the burnt flints selected for TL dating in order to tease apart their potential effects upon the obtained ages. They showed that "abrupt" dose variations (at a 10 cm scale) were significantly correlated with the gamma dose rate received by the flints.

Our present dating program at Tabun Cave was undertaken together with detailed sedimentological analysis of the exposed sections of Jelinek's former excavation (Friesem et al., 2021). Sediment samples (n=9) were collected for mineralogical analysis and direct dating using luminescence of polymineral fine grains, applied at the cave for the first time. The post-infrared infrared stimulated luminescence (pIRIR) protocol at 290°C (e.g., Thiel et al., 2011) was chosen as a suitable technique considering the presumed antiquity of the sediments and the expectation that the quartz grains had reached dose saturation. Unlike the conventional IRSL signal measured at 50°C, the post-IR IRSL signal suffers from less fading and is based on the signal measured at 290°C obtained after an IRSL bleach at 50°C and a preheat at a high temperature (≥300°C).

To gain critical insight into variation in dose rates, the level of diagenesis in the sampled sediment was assessed using the well-established method of Fourier transform infrared (FTIR) spectroscopy (Weiner and Goldberg, 1990; Goldberg et al., 2022). FTIR has often been used to understand diagenetic processes and assess the preservation state of archaeological assemblages.

The age results provided by this study are of relevance to evaluating two main issues of chronological and evolutionary significance: (1) The timing of the transition between the

Acheulo-Yabrudian of the late LP and the MP; and (2) the timing of the end of the early MP and the beginning of the Tabun C phase of the mid-MP.

2. Tabun Cave

Tabun Cave is located on the western slope of Mount Carmel, facing the coastal plain (Fig. 1a). The cave contains a 25 m deep accumulation of archaeological sediments, encompassing layers spanning from the LP to the MP (Fig. 1b-c and Fig. S1). The site was first excavated by D.A.E. Garrod between 1929 and 1934, who divided the massive sequence into seven layers: Layers G–F at the bottom are attributed to the LP Acheulian culture, Acheulo-Yabrudian Layer E marking the late LP, and Layers D–B assigned to the MP (Garrod and Bate, 1937). Subsequently, A. Jelinek's excavations between 1967 and 1971 concentrated on the middle part of Garrod's sequence, ranging from the MP Layer C down to the LP Layer E of the Acheulo-Yabrudian (Jelinek et al., 1973). A. Ronen later excavated the very lowest LP layers, equivalent to Garrod Layers G–F, as well as different parts of Layer E in 1975–2003 (Ronen et al., 2011). Recently initiated excavations by M. Weinstein-Evron, R. Shimelmitz and I. Hershkovitz, focus on the uppermost part of the sequence (Garrod's Layer B), which has not been excavated since 1934.

The almost century-long research at the cave has encompassed contributions to delineating the cultural divisions of the Near Eastern Palaeolithic (e.g., Garrod, 1962; Copeland, 1975), the reconstruction of long-term environmental changes, including geological, botanical and zoological proxy records (e.g., Bate, 1937; Jelinek et al., 1973; Friesem et al., 2021; Lev et al., 2023), technological evolution (e.g., Garrod and Bate, 1937; Jelinek, 1982, 1990; Ronen et al., 2011; Shimelmitz et al., 2020), and the changing modes of human occupation and fire use (e.g., Albert et al., 1999; Meignen et al., 2006; Shimelmitz et al., 2014; Kuhn et al., 2018; Kuhn and Stiner, 2019).

The human remains of the cave, retrieved from Garrod's excavation (McCown and Keith, 1939), are of great importance due to the presence of several hominin populations, especially within the MP layers. The most complete fossil (Tabun C1) is that of a female burial found at the upper part of Layer C, whose attribution to a specific phase of the MP at the cave remains controversial (Garrod and Bate, 1937; Bar-Yosef and Callander, 1999). It is usually classified as Neanderthal (Tillier, 2005). Below it, at the base of Layer C, a human mandible (Tabun C2) was attributed to *Homo sapiens* (Rak, 1998) or archaic *Homo* (Harvati and Lopez, 2017).

While Garrod's work paved the foundations of our understanding of the site, it is Jelinek's research that significantly enhanced the resolution of investigation: What Garrod initially divided into three layers (C–E), Jelinek further divided into a set of 14 units and 86 layers (Beds; 1–85, 90): Unit I aligns with Layer C of the mid-MP and encompasses Beds 1–26, Units II–IX correspond to Layer D of the early MP, and Units X–XIV correspond to Layer E of the Acheulo-Yabrudian (Jelinek, 1982) (Fig. 1c).

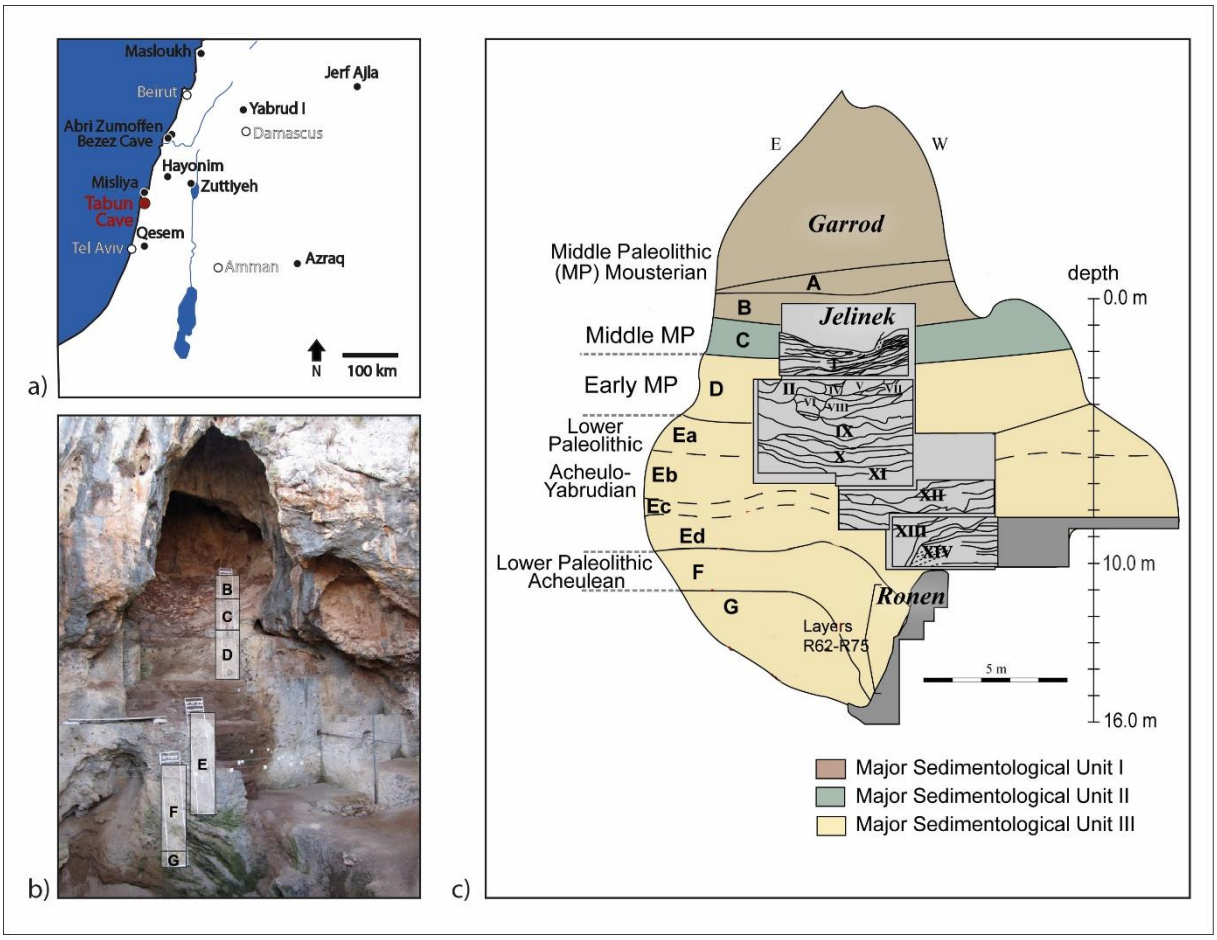

Fig. 1. Location of Tabun Cave (in red) (a), view of the cave with Garrod's layers (b), and the stratigraphic sequence with Garrod's layers (A to G; Garrod and Bate, 1937) and the later excavations by Jelinek (1982) (I to XIV) and Ronen's layers R62 to R75 (Ronen et al., 2011) (c). For a detailed view of Units I and II, the reader is referred to Fig. S1.

The division of the sequence into three Major Sedimentological Units (MSUs) by Jelinek et al. (1973) has been recently refined by Friesem et al. (2021). MSU III forms the major part of the cave's accumulation and runs from its base to the end of Garrod's Layer D. It is composed primarily of aeolian sediments, consisting mainly of sand and silt, with the proportion of the latter increasing towards the top of the sequence. The sediments are

characterised by extensive diagenesis. MSU II is equivalent to Garrod's Layer C and consists of a series of laminae varying in colour and composition. Its components include terra rossa soil, which originated from an opening of the cave's chimney, and massive amounts of bat and bird guano at various stages of diagenesis. Evidence of human occupation, especially the use of fire, is abundant at the lower part of MSU II. The recent micromorphological analysis of the MP section also offered some refinement for the boundary between Units I-II and identified some differences between the western and eastern profiles. While in the eastern profile the lower part of Unit I reaches Bed 25, in the western profile Bed 22 forms the lowest part of this unit. The layer defined by Jelinek as Bed 23 at the western profile and originally assigned by him to Unit I, was now found to be parallel to the upper part of Unit II and to form part of MSU III (Friesem et al. 2021).

3. Material and Methods

3.1. Sediment samples

A set of nine sediment samples were subjected to this research retrieved from both the east and west sections of Jelinek's excavation (Table 1). They include: (1) three samples from the base of Unit I (Layer C), ranging from Beds 19-22; (2) a single sample from Bed 23 west, which was formerly assigned by Jelinek (1982) to the base of Unit I at the western section but recent micromorphological research shows it is part of Unit II (Upper Layer D) (Friesem et al., 2021); (3) two samples from Unit II, Beds 27 and 28 (Upper Layer D); (4) two samples from Unit IX (Lower Layer D) including Beds 63-64 on the western section and Bed 63 on the eastern section; and (5) a single sample from Unit X, Bed 72 (Upper Layer E) which is among the uppermost LP occupation layers, formerly assigned as transitional LP-MP.

Sediment samples were collected at night from fresh sections and kept in light-proof bags. Al_2O_3:C dosimeters were placed in the section, next to the sampling location, for a year to record the gamma dose rate. The sediments were prepared in the luminescence laboratory under subdued red light and measurements were performed at Archéosciences Bordeaux (Pessac, France). The polymineral 4-11 μm fraction was extracted by decantation using Atterberg according to Stokes's law. The organic matter and carbonates were eliminated using H_2O_2 (30%) and HCl (10%), respectively.

3.2. Luminescence

Multigrain measurements were conducted using the single aliquot regeneration (SAR) protocol (Murray and Wintle, 2000) and the $pIRIR_{290}$ protocol was applied. For this purpose, a thin and homogeneous layer of grains was deposited on cups and measured on a Lexsyg Smart TL/OSL reader (Richter et al., 2015) following the protocol displayed in Table 2. Infrared laser diodes were used for stimulation (power density: 30 $mW \cdot cm^{-2}$) and the signal was detected with a combination of optical filters (Schott BG 39-3 mm; AHF Brightline HC 414/46-3.5 mm).

As the $pIRIR_{290}$ signal does not bleach as fast as the ones measured at lower temperatures (e.g., Buylaert et al., 2011), a residual dose may remain even after several days of bleaching (Kars et al., 2014). To assess the residual dose as a function of bleaching time, the TAB 5 sample was bleached in a solar simulator (Hönle 500) for 4, 24, 48 and 120h (three aliquots each). The residual doses range from ~20 Gy (4h bleaching) to ~8 Gy (120h) (Fig. S2). The measured residual doses are low compared to the accumulated doses and, since it is not possible to precisely determine the level of bleaching at the time of deposition, these residual doses were not subtracted from the measured equivalent doses.

TAB #	Depth (m)	Layer (Garrod and Bate, 1937)	Unit (Jelinek, 1982)	Bed (Jelinek, 1982)	Section
15	-2.73	C	I	19	E
3	-1.97	C	I	20	W
4	-2.12	C	I	21-22	W
5	-2.25	D (upper, formerly C)	II*	23 west	W
6	-3.56	D (upper)	II	27	E
17	-3.87	D (upper)	II	28	E
12	-4.36	D (lower)	IX	63-64	W
18	-4.88	D (lower)	IX	63	E
10	-5.73	E upper	X (transitional)	72	W

Table 1. List of the sediment samples analysed in this study. The match between the different layers, units and beds are presented in Fig. 1 and Fig. S1. *While Bed 23 west was originally defined by Jelinek as the base of Unit I at the western section, the new geoarchaeological research found it to form the upper part of Unit II (Friesem et al. 2021).

The preheat (PH) temperature used for the measurements was selected based on the dose recovery tests (DRT) conducted on sample TAB 5 using three different PH temperatures of 250°C, 300°C and 320°C, and using two techniques:

1) Adding a dose (142 Gy) on the top of the natural dose (unbleached aliquot). The recovery ratios were calculated by normalising the recovered value to the sum of the

given irradiation dose and the mean equivalent dose measured on natural aliquots (5 to 15 aliquots depending on the PH temperature);

2) Bleaching the sample for 4h, adding a dose (568 Gy) similar to those measured in the oldest samples (602 Gy), and subtracting the residual dose measured after 4h. The recovery ratios were calculated by subtracting the residual dose from the recovered value and normalised by the given dose.

The best recovery ratios were obtained with a PH temperature of 300°C (0.99 ± 0.04 when adding a dose on natural) and 0.89 ± 0.02 (when adding a dose after a 4h bleach). At 250°C, the recovery ratios were overestimated (1.32 ± 0.03, added dose on natural, and 1.31 ± 0.07, added dose after 4h bleach), and underestimated at 320°C (0.91 ± 0.02, added dose on natural, and 0.77 ± 0.05 added dose after 4h bleach). Given the relatively high temperature of the second stimulation step (290°C), which selectively targets more stable electron traps, it was assumed that the fading rate of the measured $pIRIR_{290}$ signal was close to zero and, if this was not the case, this could have led to an underestimation of the accumulated dose. It should also be noted that, if such an underestimation exists, it is partly offset by the fact that no residual dose was subtracted.

Step	**Treatment**
1	Given dose
2	Preheat (300°C for 60 s)
3	IR stimulation for 200 s at 50°C
4 (L_x)	IR stimulation for 200 s at 290°C
5	Given test dose
6	Preheat (300°C for 60 s)
7	IR stimulation for 200 s at 50°C
8 (T_x)	IR stimulation for 200 s at 290°C
9	IR stimulation for 60 s at 325°C
10	Return to 1

Table 2. $pIRIR_{290}$ SAR measurement protocol applied to polymineral fine grains.

For each sediment sample, the alpha and beta dose rate was derived from its U, Th and K contents measured with a laboratory gamma-ray spectrometer equipped with a high-resolution, broad energy Ge (BEGe) detector. The dosimeters were analysed using the procedure described in Kreutzer et al. (2018b). $pIRIR_{290}$ ages were calculated with the 1 σ error range taking into account beta absorption factors of 0.015 (U), 0.020 (Th) and 0.002 (K) (Guérin

et al., 2012); alpha attenuation factors of 0.85 (U) and 0.87 (Th) (Brennan et al., 1991); an α-value of 0.067 ± 0.012 (Kreutzer et al., 2018a) and a K-content assumed in the feldspar grains of 12 ± 1%. A value of 70 ± 10 µGy/a was calculated for the cosmic dose rate, based on the equation of Prescott and Hutton (1988). The water content was assessed to be 15% based on Mercier et al. (1995b) (2-24% measured).

The luminescence data were processed using Analyst v. 4.57 (Duller, 2007): The signal was integrated using the first 5 s and background was subtracted from the last 50 s. The following criteria were applied for the data selection: a recycling ratio limit of 10%; a recuperation < 5% of the natural signal; a maximum test dose error of 10%; and a test dose signal > 3 sigma above background. For each sample, 5 to 7 aliquots were measured following the SAR protocol (Table 2) and allowed to obtain normalised dose response curves (DRC). These data were fitted with an exponential function (Fig. S3a) in order to construct a global growth curve (GGC; Fig. S3b), on which L_n/T_n signals measured for 15 additional aliquots were plotted to compute individual equivalent doses (D_e) (Fig. S4). The central age model (CAM, Galbraith et al., 1999) was used to calculate the equivalent dose for each sample.

3.3. Fourier transform infrared (FTIR) spectroscopy

The mineral composition of each sediment sample was determined using FTIR spectroscopy. Measurements were carried out at the Kimmel Center for Archaeological Science (Weizmann Institute of Science, Rehovot, Israel) using a Thermo Scientific Nicolet iS5 spectrometer in 32 scans at 4 cm^{-1} resolution in the 4000-400 cm^{-1} spectral range. The sediment was mixed with KBr (~40 mg) and pressed into a 7-mm pellet. The spectra were analysed using OMNIC v. 9.6 and mineral identification was based on the Kimmel Center for Archaeological Science Infrared Standards Library (Weizmann Institute of Science), available at https://centers.weizmann.ac.il/kimmel-arch/infrared-spectra-library.

4. Results and discussion

As expected for polymineral fine grains, the distribution of equivalent doses is homogeneous for most of the samples, except for TAB 12 and 10 whose distribution appears scattered. However, considering their error range, the D_e overlap (Fig. S4). Dosimetric data and $pIRIR_{290}$ ages are presented in Table 3 and Fig. 2.

TAB #	Bed (layer)	*n* GGC	*n* L_n/T_n	D_e (Gy)	Dose rate (µGy/a)				
					Alpha	Beta	Gamma + cosmic	Total	Age (ka)
15	19 (C)	5	15	264 ± 3	245 ± 33	757 ± 12	355 ± 18	1357 ± 38	195 ± 16
3	20 (C)	7	15	232 ± 2	141 ± 18	444 ± 13	620 ± 32	1205 ± 38	192 ± 14
4	21-22 (C)	5	15	384 ± 5	433 ± 56	789 ± 16	663 ± 33	1885 ± 66	204 ± 18
5	23west (D upper)	5	15	442 ± 5	499 ± 64	905 ± 18	613 ± 32	2017 ± 73	219 ± 20
6	27 (D upper)	5	15	373 ± 4	346 ± 46	620 ± 16	456 ± 22	1422 ± 53	262 ± 23
17	28 (D upper)	5	15	472 ± 5	703 ± 93	1060 ± 11	610 ± 29	2373 ± 98	199 ± 19
12	63-64 (D lower)	6	15	602 ± 22	641 ± 83	923 ± 10	525 ± 25	2088 ± 86	288 ± 29
18	63 (D lower)	5	15	523 ± 7	693 ± 90	1570 ± 18	504 ± 24	2766 ± 94	189 ± 17
10	72 (E upper)	6	15	499 ± 19	516 ± 67	728 ± 11	638 ± 28	1882 ± 72	265 ± 26

Table 3. Luminescence and dose rate data, and ages obtained at Tabun Cave. The beta dose rate includes the internal (19 ± 2 µGy/a) and external contributions. The cosmic dose rate was estimated to 70 ± 10 µGy/a and added to the gamma dose rate measured by Al_2O_3:C dosimeters. The beta dose rate was calculated from U, Th and K content measured in the sediment and presented in Table S1. *n* GGC = number of aliquots measured with the SAR protocol that passed criteria and used to construct the GGC. *n* L_n/T_n = number of L_n/T_n signal measured and plotted on the GGC. Note that the D_e were calculated using both SAR D_e and interpolated L_n/T_n.

The $pIRIR_{290}$ ages range cover the sequence from Bed 72, the very upper LP, for which an age of 265 ± 26 ka was obtained, to layer C, Unit I, Bed 19 of the mid-MP, which provided an age of 195 ± 16 ka; they increase overall with depth and are in agreement with the previously obtained TL ages at 1 σ (Fig. 2). However, we observe two ages incongruent with their stratigraphic position, one at the base of the sequence where Bed 63-64 is dated to 288 ± 29 ka (TAB 12) and 189 ± 17 ka (TAB 18), and another higher in the stratigraphy where Bed 27 is dated to 262 ± 23 ka (TAB 6) while the underlying Bed 28 gave an age of 199 ± 19 ka (TAB 17).

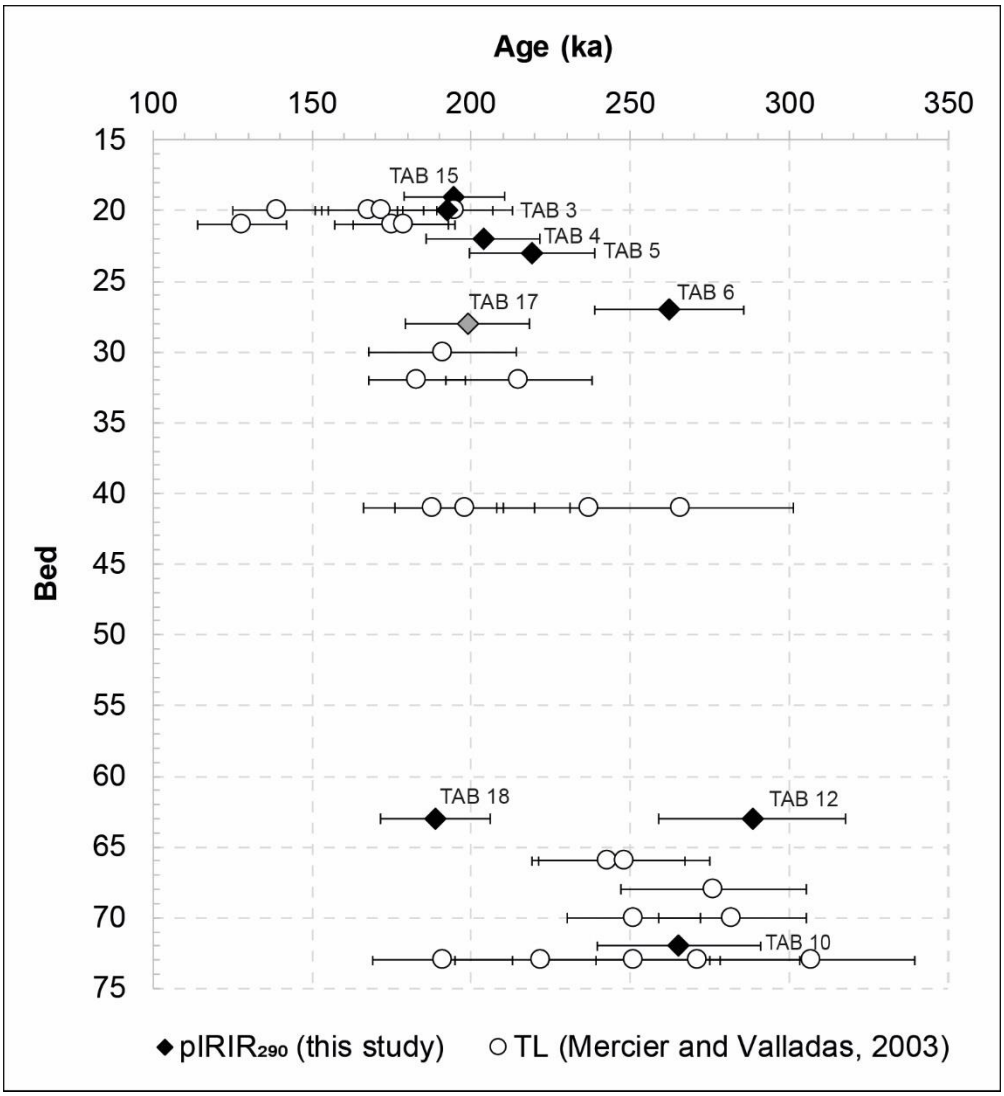

Fig. 2. Comparison of $pIRIR_{290}$ ages with published TL results from Mercier and Valladas (2003). The black diamonds refer to the samples where phosphates have been identified with FTIR.

To explain these results, it is noted that the dose rate is highly variable from one bed to the other, but also within the same bed (Fig. 3). This is especially apparent in the case of Beds 27 and 28, in which the beta dose rate ranges from 620 ± 16 (TAB 6) to 1060 ± 10 µGy/a (TAB 17) and within Bed 63-64, in which it ranges from 923 ± 10 (TAB 12) to 1570 ± 18 µGy/a (TAB 18). These variations are directly related to differential contents in radioelements, U for Bed 27-28 and K for Bed 63/64 (Table S1 and Fig. 3). Of note here is sample TAB 5 that was also retrieved from Unit II in upper Layer D, yielding a date of 219 ± 20, not much different from that of TAB 17. In the case of the difference between TAB 12 (Beds 63/64) and TAB 18 (Bed 63), it may have to do with the fact that the two samples were taken from different profiles evincing different sedimentological regimes. While the western profile (the provenance of TAB

12) demonstrates clear stratification of Unit IX underlying Units VIII and VII, in the eastern profile (the provenance of TAB 18), Unit IX is covered by lenses of sediments, termed Units VI and IV, and the much younger Unit II (Fig. 1c). A part of the original deposits that probably accumulated in this part of the cave seems to have washed away.

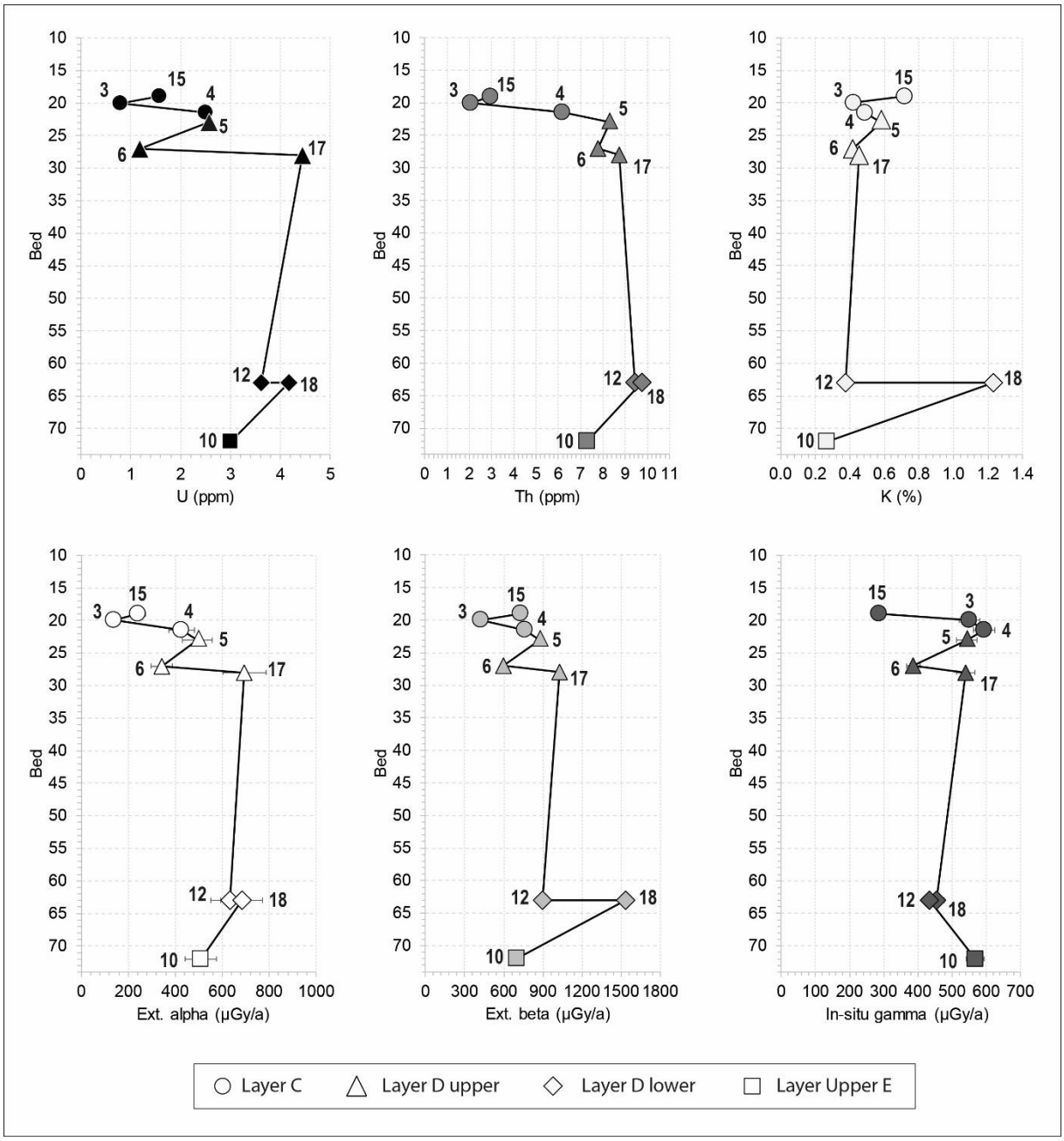

Fig. 3. Graphic representation of U, Th and K content (top) and alpha, beta and gamma dose rate (bottom) in the different beds.

Moreover, it has been shown that changes in the mineral assemblages at a small scale due to geochemical conditions may induce significant variations in the dose rate (Mercier et al.,

1995a; Weiner et al., 2002). In particular, when organic material is present in archaeological layers and breaks down (e.g., guano, fossil bones and teeth), phosphates are released and the pH decreases. Consequently, carbonates, particularly the more soluble forms such as aragonite and calcite, dissolve in acidic water. As a result, authigenic phosphates may form from the reaction between the original phosphates and calcium ions. The nature of the resulting secondary minerals will depend on the pH and the phosphate concentration (Fig. 1 in Weiner et al., 2002): the initial formation is carbonate hydroxyapatite, followed by more stable minerals such as crandallite, montgomeryite, leucophosphite, and taranakite.

At Tabun Cave, sources of phosphates were present as a result of human activity, particularly hunted animal bones, which were dissolved due to organic acids (derived from bat guano, plant decay, humic acid, etc.), or slightly acidic water, and released phosphate ions in solution that, upon reacting with calcium ions, promoted the formation of secondary carbonate hydroxyapatite. Other less soluble authigenic phosphates (e.g., montgomeryite, crandallite) are also found in parts of the sequence where little or no calcite is preserved (Goldberg and Nathan, 1975).

Friesem et al. (2021), who studied the Tabun stratigraphy in detail using FTIR and micromorphology among other techniques, demonstrated the presence of calcite, transformed clay (showing alteration attributed to chemical weathering), carbonate hydroxyapatite coming from the decomposition of guano, ashes and bones, heat-altered and unheated clay minerals, and authigenic minerals such as crandallite, leucophosphite, and montgomeryite. Our FTIR measurements were performed on the dated sediment samples used for the gamma spectrometry analyses in order to investigate their mineral composition, to assess their state of preservation and better understand dose rate variations (i.e., variations in radioelement contents among samples located within the same bed or in closely adjacent beds). The spectra are provided in Fig. S5. We observe the presence of calcite in small quantity in most of the samples (peaks at 1420, 876, 712 cm^{-1}), quartz (1080, 797-779, 695 cm^{-1}), clay minerals (3420, 470 cm^{-1}), and authigenic phosphates (PO) (Table 4 and Fig. S5e). In the case of TAB 3, the presence of the phosphate bands v_3 (1035 cm^{-1}) and v_4 (604 and 567 cm^{-1}) suggests that the sediment is entirely phosphatised (Fig. S5b), similar to TAB 15, where v_3 and v_4 are associated with clay minerals and quartz (Fig. S5a).

The presence of calcite in most of the samples indicates that the sediment did not undergo significant alterations, calcite being one of the less stable polymorph of $CaCO_3$ after aragonite, except if this calcite is the result of a more recent event. However, the presence of montgomeryite (at 590 cm^{-1}), associated with little calcite (i.e., TAB 5 and 6) (also observed

by Goldberg and Nathan, 1975), suggests that the sediment suffered localised diagenetic processes, just as the phosphatised sediments of TAB 15 and 3. The transformation of the mineral assemblages over time indicates that the dose rate (especially the beta component whose impact is limited to a few millimetres) may not have remained constant at the scale of the dated grains, which in turn could have impacted the age results.

In Fig. 2, $pIRIR_{290}$ ages are represented as a function of depth (beds). One of the samples in which authigenic phosphates have been identified (black diamonds), TAB 18, appears to be younger. Nonetheless, this anomaly does not seem to affect significantly other samples, such as TAB 15, 3, 4, 5, 12 and 10, whose ages are stratigraphically consistent with the age of TAB 17, which appears to be well-preserved.

TAB #	Calcite	Quartz	Clay minerals	Authigenic phosphates	Transforming clays
15 (C)	+	+	+	+	
3 (C)	+	+		+	
4 (C)	+	+	+	+	
5 (D upper)	+	+		+	
6 (D upper)	+	+	+	+	
17 (D upper)	+	+	+		
12 (D lower)	+	+		+	+
18 (D lower)	+	+	+	+	
10 (E upper)	+	+		+	+

Table 4. Mineral identification in the dated samples. The FTIR spectra are available in Fig. S5. Among the authigenic phosphates, carbonate hydroxyapatite was identified in TAB 15, 3, 4, 12, 18, 10 and montgomeryite in TAB 5 and 6.

Moreover, we cannot exclude the possibility that part of the discrepancy between the age results is related to the residual dose, which may not have been the same for all samples (e.g., TAB 6 and 12), even though, as mentioned earlier, this effect is likely limited given the relative value of the residual dose compared to the mean equivalent dose. We cannot also rule out the possibility that fine sediments may have been episodically washed through the chimney from older soils present on the plateau above the cave, without undergoing sufficient bleaching during this transport.

In spite of all these points, which are difficult to quantify and partly inaccessible today, our $pIRIR_{290}$ results are globally in agreement at 1σ with the TL ages obtained on burnt flints and updated by Mercier and Valladas (2003). Exception is sample TAB 6 (Fig. 2), although one notices that the TL ages are also highly variable within the same layer. For example, in Bed 41

(Unit V), the age range covers up to 100 ka. Mercier and Valladas (2003) observed spatial variations of the gamma dose rate correlated with high U and K content measured locally in sediment samples taken at relevant locations in this bed. This led to significant differences (15 to 20%) between the dose recorded by the dosimeters and those derived from U, Th and K contents. In Unit IX (Beds 66-68), where variations of the gamma dose rate were also observed, the bones were completely dissolved as a result of strong geochemical changes. In the case of burnt flints, for which the gamma dose rate can be a significant fraction of the dose rate, such variations may have impacted the ages. In Hayonim Cave (Fig. 1a), Weiner et al. (2002) identified three main mineral assemblages: one with calcite-dahllite, one mainly composed of authigenic phosphates such as montgomeryite, leucophosphite and siliceous aggregates (containing a high level of K; Schiegl et al., 1994), and another with altered clays. Mercier et al. (1995a) calculated the dose rate from U, Th and K content measured in the first two types of these assemblages. They showed that the dose rate in the assemblage comprising authigenic phosphate can reach values up to ca. 1200 µGy/a, which is almost twice the dose in the calcite-dahllite assemblage (ca. 500 µGy/a). A similar observation has recently been made in Galería, in the Sierra de Atapuerca (Spain), where Campaña et al. (2023) proposed that the source of discrepancies between TT-OSL, ESR/U-series and paleomagnetism ages is the presence of phosphates (crandallite), which lead to an underestimation of the ages obtained by trapped-charge dating methods. Interestingly, in Arago Cave (France), Han et al. (2010) showed that ESR/U-series ages obtained from fossil enamel are older in the phosphatised area than in the unaltered one.

In a study of cave diagenesis, including samples from Hayonim Cave, Karkanas et al. (2000) suggested that diagenesis may happen soon after sediment deposition, and may occur at the surface or just below it. If that was the case in Tabun Cave, then the feldspars from the dated polymineral fractions may have been exposed to the current dose rate during most of the burial time and the diagenetic processes may not have significantly affected the age results. However, if this was not the case, diagenesis within the sediments could be a major limitation for trapped-charge dating methods in general, especially when diagenesis impacts both short-range (beta) and long-range (gamma) particles, which must be considered when dating grains instead of large artefacts, like flints.

Our study supports the use of FTIR as a pre-screening method, i.e., when it can be applied in the field before collecting samples for trapped-charge dating. Indeed, mineralogical analyses of the sediments give useful insights into spatial variation in the magnitude and nature of diagenetic processes, which is particularly relevant for reconstructing the dose rate for teeth

and burnt flints dated by ESR and TL, respectively. For instance, for samples that were not found in the immediate vicinity of the sections, correlating the contexts for both samples and dosimetry based on the mineral assemblages is essential to reconstruct the gamma dose rate and provide reliable ages (Weiner et al., 2002).

5. Conclusions

Investigating the nature of the mineral assemblages in potentially altered contexts is essential to target the best location for dating and understand the spatial variation of the dose rate, particularly in cave sites. For this purpose, FTIR spectroscopy gives useful indications for the interpretation of dosimetric data, and especially for TL and ESR dating, in order to correlate the mineral assemblages present in the context of the sample and those in which the dosimeters are inserted.

Luminescence ($pIRIR_{290}$) ages have been obtained for a series of nine sediment samples from Tabun Cave. They indicate that the sediments taken from Jelinek's Units X–I were deposited between 265 ± 26 ka (Bed 72) and 195 ± 16 ka (Bed 19).

Regarding the transition between the LP and MP of the Levant, the earliest age obtained in the current analysis is from Bed 72. This layer is placed at the base of Jelinek's Unit X (Beds 70–72). While Jelinek (1982) defined this unit as "transitional" between the LP and MP, recent analysis by Shimelmitz et al. (2021) suggested that Bed 72 better represents the very end of the Acheulo-Yabrudian complex and the termination of the LP in the Tabun sequence. The age of 265 ± 26 ka obtained for Bed 72 is statistically indistinguishable from the mean TL age results of both Unit X (267 ± 22 ka) and Unit XI (264 ± 28 ka) (Mercier and Valladas, 2003). This early age, which indicates the end of the LP in Tabun, aligns with other dating results from the Levant, such as at Misliya Cave, which provided ages as early as 250 ka for the Acheulo-Yabrudian Complex (Valladas et al., 2013). However, this series of ages does not align with other dating results from Qesem Cave that yielded ages as late as 200 ka (Mercier et al., 2013; Falguères et al., 2016).

The age range for Beds 63-64 at the upper part of Unit IX is 288 ± 29 to 189 ± 17 ka. The initial appearance of Mousterian industries characterised by the Levallois technology should fall within this range. Building on further reinforcing evidence from the intensively dated early MP layer at Misliya (Valladas et al., 2013; Hershkovitz et al., 2018), we propose an earlier onset of this phase (earlier than 250 ka). Here however, future dating of Beds 62–69

(Unit IX) may shed further light on the antiquity of the early MP in the Levant. Given these limitations, our present study brackets the LP–MP transition between 265 ± 26 ka and 288 ± 29 ka, lending more credibility to the generally proposed age of ca. 250 ka for this transition (Valladas et al. 2013) than much younger estimates.

The end of the early MP (Layer D) should correspond to the ages of Bed 23 west (219 ± 20 ka) and Bed 28 (199 ± 19 ka) of Jelinek's Unit II. The early age of 262 ± 23 ka obtained from Bed 27 of Jelinek's Unit II seems unlikely within the overall distribution of ages. Excluding this date, the ages from the lower part of mid-MP Layer C range from 204 ± 18 ka to 192 ± 14 ka, giving a weighted mean age of 196 ± 9 ka to the lower part of Layer C/Unit I. While there is ongoing debate regarding the precise timing of the transition between the early and middle phases of the MP, with estimates ranging between 140-160 ka (e.g., Valladas et al., 2013; Shea, 2014; Goder-Goldberger and Bar-Matthews, 2019; Zaidner et al., 2021; Wojtczak and Malinsky-Buller, 2022), our results support the early limit of this range, and imply an even older age for this transition. Nonetheless, one must keep in mind that the lack of a clear boundary between the middle and late phases of the MP across Levantine sites has been acknowledged (e.g., Shea, 2014; Oron et al., 2024), and this may also be the case of the boundary between its early and middle phases.

Lastly, in case the beginning of the MP in the Levant is indeed contemporaneous with the arrival of *Homo sapiens* in the region, as commonly argued (Hershkovitz et al., 2018; Meignen and Bar-Yosef, 2020; Zaidner and Weinstein-Evron, 2020), then this pivotal event may have occurred earlier than commonly believed (as well as any transitional processes involved; Shimelmitz et al., 2021). Furthermore, the newly obtained ages may place the Tabun C2 mandible, found at the base of Layer C, within an especially early timeframe ranging between 204 ± 18 ka to 192 ± 14 ka. In case the identification of the mandible as early *Homo sapiens* (Rak, 1998) holds, then this specimen, together with Misliya-1, are among the oldest fossils of *Homo sapiens* outside of Africa (e.g., Hershkovitz et al., 2018; Harvati et al., 2019).

Acknowledgments

In its early phase, this work has been funded by the LaScArBx (ANR-10-LABX-52), the Gerda Henkel Foundation (AZ F/35/16) and the Israel Science Foundation (1955/2016). This research benefited also from the scientific framework of the University of Bordeaux's IdEx "Investments

for the Future" program / GPR "Human Past". We thank E. Boaretto (Weizmann Institute of Science) for accessing the FTIR spectrometer at The Helen and Martin Kimmel Center and M.B. Toffolo (CENIEH) for help in interpreting FTIR spectra. We also thank D. Friesem (University of Haifa) who has been working on the geoarchaeology of Tabun Cave, C. Tribolo, P. Urbanová and E. Rafins (Archéosciences Bordeaux) for useful advices and help with measurements. We thank the anonymous reviewer as well as the guest editor for their constructive comments that improved this manuscript.

References

Albert, R.M., Lavi, O., Estroff, L., Weiner, S., Tsatskin, A., Ronen, A., Lev-Yadun, S., 1999. Mode of Occupation of Tabun Cave, Mt Carmel, Israel During the Mousterian Period: A Study of the Sediments and Phytoliths. Journal of Archaeological Science 26, 1249-1260.

Bar-Yosef, O., 1994. The Lower Paleolithic of the Near East. Journal of World Prehistory 8, 211-265.

Bar-Yosef, O., Callander, J., 1999. The woman from Tabun: Garrod's doubts in historical perspective. Journal of Human Evolution 6, 879-885.

Barzilai, O., Abulafia, T., Shemer, M., May, H., Orbach, M., Frumkin, A., Yeshurun, R., Sarig, R., Porat, N., Hershkovitz, I., 2022. Rediscovering Geula Cave: A Middle Paleolithic cave site in northern Mt. Carmel, Israel. Quaternary International 624, 181-197.

Bate, D.M.A., 1937. Palaeontology: the fossil fauna of the Wady el-Mughara caves, in: Garrod, D.A.E., Bate, D.M.A. (Eds.), The Stone Age of Mount Carmel. Vol. I. Excavations at the Wadi Mughara. Clarendon Press, Oxford, pp. 137–240.

Brennan, B.J., Lyons, R.G., Phillips, S.W., 1991. Attenuation of alpha particle track dose for spherical grains. International Journal of Radiation Applications and Instrumentation. Part D. Nuclear Tracks and Radiation Measurements 18, 249-253.

Buylaert, J.-P., Thiel, C., Murray, A., Vandenberghe, D., Yi, S., Lu, H., 2011. IRSL and post-IR IRSL residual doses recorded in modern dust samples from the Chinese Loess Plateau. Geochronometria 38, 432-440.

Campaña, I., Benito-Calvo, A., Pérez-González, A., Ortega, A.I., Álvaro-Gallo, A., Miguens-Rodríguez, L., Iglesias-Cibanal, J., de Castro, J.M.B., Carbonell, E., 2023. Reconstructing depositional environments through cave interior facies: The case of Galería Complex (Sierra de Atapuerca, Spain). Geomorphology 440, 108864.

Copeland, L., 1975. The Middle and Upper Paleolithic of Lebanon and Syria in the light of recent research. Problems in prehistory: North Africa and the Levant, 317-350.

Duller, G.A., 2007. Assessing the error on equivalent dose estimates derived from single aliquot regenerative dose measurements. Ancient TL 25, 15-24.

Falguères, C., Richard, M., Tombret, O., Shao, Q., Bahain, J.J., Gopher, A., Barkai, R., 2016. New ESR/U-series dates in Yabrudian and Amudian layers at Qesem Cave, Israel. Quaternary International 398, 6-12.

Friesem, D.E., Shahack-Gross, R., Weinstein-Evron, M., Teutsch, N., Weissbrod, L., Shimelmitz, R., 2021. High-resolution study of Middle Palaeolithic deposits and formation processes at Tabun Cave, Israel: Guano-rich cave deposits and detailed stratigraphic appreciation of Layer C. Quaternary Science Reviews 274, 107203.

Galbraith, R.F., Roberts, R.G., Laslett, G.M., Yoshida, H., Olley, J.M., 1999. Optical dating of single and multiple grains of quartz from Jinmium rock shelter, northern Australia: Part I, experimental design and statistical models. Archaeometry 41, 339-364.

Garrod, D., 1962. The Middle Palaeolithic of the Near East and the problem of Mount Carmel man. The Journal of the Royal Anthropological Institute of Great Britain and Ireland 92, 232-259.

Garrod, D.A., Bate, D.M.A., 1937. The Stone Age of Mt Carmel, Excavations at the Wadi El-Mughara, vol. 1. Clarendon Press, Oxford.

Goder-Goldberger, M., Bar-Matthews, M., 2019. Novel chrono-cultural constraints for the Middle Paleolithic site of Rosh Ein Mor (D15), Israel. Journal of Archaeological Science: Reports 24, 102-114.

Goldberg, P., Macphail, R.I., Carey, C., Zhuang, Y., 2022. Practical and theoretical geoarchaeology. John Wiley & Sons.

Goldberg, P.S., Nathan, Y., 1975. The phosphate mineralogy of et-Tabun cave, Mount Carmel, Israel. Mineralogical Magazine 40, 253-258.

Gopher, A., Ayalon, A., Bar-Matthews, M., Barkai, R., Frumkin, A., Karkanas, P., Shahack-Gross, R., 2010. The chronology of the late Lower Paleolithic in the Levant based on U–Th ages of speleothems from Qesem Cave, Israel. Quaternary Geochronology 5, 644-656.

Groucutt, H.S., Scerri, E.M.L., Stringer, C., Petraglia, M.D., 2019. Skhul lithic technology and the dispersal of Homo sapiens into Southwest Asia. Quaternary International 515, 30-52.

Grün, R., Stringer, C., 2000. Tabun revisited: revised ESR chronology and new ESR and U-series analyses of dental material from Tabun C1. Journal of Human Evolution 39, 601-612.

Grün, R., Stringer, C., McDermott, F., Nathan, R., Porat, N., Robertson, S., Taylor, L., Mortimer, G., Eggins, S., McCulloch, M., 2005. U-series and ESR analyses of bones and teeth relating to the human burials from Skhul. Journal of Human Evolution 49, 316-334.

Guérin, G., Mercier, N., Nathan, R., Adamiec, G., Lefrais, Y., 2012. On the use of the infinite matrix assumption and associated concepts: A critical review. Radiation Measurements 47, 778-785.

Han, F., Falguères, C., Bahain, J.J., Shao, Q., Duval, M., Lebon, M., Garcia, T., Dolo, J.M., Perrenoud, C., Shen, G.J., de Lumley, H., 2010. Effect of deposit alterations on the dating of herbivorous teeth from Arago cave by the ESR–U-series method. Quaternary Geochronology 5, 376-380.

Harvati, K., Lopez, E.N., 2017. A 3-D Look at the Tabun C2 Jaw, in: Marom, A., Hovers, E. (Eds.), Human Paleontology and Prehistory: Contributions in Honor of Yoel Rak. Springer International Publishing, Cham, pp. 203-213.

Harvati, K., Röding, C., Bosman, A.M., Karakostis, F.A., Grün, R., Stringer, C., Karkanas, P., Thompson, N.C., Koutoulidis, V., Moulopoulos, L.A., Gorgoulis, V.G., Kouloukoussa, M., 2019. Apidima Cave fossils provide earliest evidence of *Homo sapiens* in Eurasia. Nature 571, 500-504.

Hershkovitz, I., Weber, G.W., Quam, R., Duval, M., Grün, R., Kinsley, L., Ayalon, A., Bar-Matthews, M., Valladas, H., Mercier, N., Arsuaga, J.L., Martinón-Torres, M., Bermúdez de Castro, J.M., Fornai, C., Martín-Francés, L., Sarig, R., May, H., Krenn, V.A., Slon, V., Rodríguez, L., García, R., Lorenzo, C., Carretero, J.M., Frumkin, A., Shahack-Gross, R., Bar-Yosef Mayer, D.E., Cui, Y., Wu, X., Peled, N., Groman-Yaroslavski, I., Weissbrod, L., Yeshurun, R., Tsatskin, A., Zaidner, Y., Weinstein-Evron, M., 2018. The earliest modern humans outside Africa. Science 359, 456-459.

Hovers, E., 2009. The lithic assemblages of Qafzeh Cave. Oxford University Press.

Jelinek, A.J., 1982. The Middle Paleolithic in the southern Levant, with comments on the appearance of modern *Homo Sapiens*, in: Ronen, A. (Ed.), The transition from Lower to Middle Paleolithic and the origin of modern man. BAR International Series, Oxford, pp. 57-101.

Jelinek, A.J., 1990. The Amudian in the context of the Mugharan tradition at the Tabun Cave (Mount Carmel), Israel, The emergence of modern humans: An archaeological perspective, pp. 81-90.

Jelinek, A.J., Farrand, W.R., Haas, G., Horowitz, A., Goldberg, P., 1973. New excavations at the Tabun Cave, Mount Carmel, Israel, 1967-1972: a preliminary report. Paléorient, 151-183.

Karkanas, P., Bar-Yosef, O., Goldberg, P., Weiner, S., 2000. Diagenesis in Prehistoric Caves: the Use of Minerals that Form In Situ to Assess the Completeness of the Archaeological Record. Journal of Archaeological Science 27, 915-929.

Kars, R.H., Reimann, T., Ankjærgaard, C., Wallinga, J., 2014. Bleaching of the post-IR IRSL signal: new insights for feldspar luminescence dating. Boreas 43, 780-791.

Kreutzer, S., Martin, L., Dubernet, S., Mercier, N., 2018a. The IR-RF alpha-Efficiency of K-feldspar. Radiation Measurements 120, 148-156.

Kreutzer, S., Martin, L., Tribolo, C., Selva, P., Mercier, N., 2018b. Environmental dose rate determination using a passive dosimeter: Techniques and workflow for α-Al_2O_3: C chips. Geochronometria 45, 56-67.

Kuhn, S.L., Shimelmitz, R., Clark, A.E., 2018. The road to differentiated land use and domestic space in the Middle Pleistocene of southwestern Asia, in: Gamble, C., McNabb, J., Pope, M. (Eds.), Crossing the human threshold. Routledge, Abingdon, pp. 43-59.

Kuhn, S.L., Stiner, M.C., 2019. Hearth and home in the Middle Pleistocene. Journal of Anthropological Research 75, 305-327.

Lev, M., Shimelmitz, R., Weinstein-Evron, M., Yeshurun, R., 2023. Paleoenvironments and climate at Nahal Me'arot (Mount Carmel, Israel) during the Middle and Late Pleistocene: The herpetofauna of Tabun Cave and el-Wad Terrace. Quaternary Science Reviews 307, 108060.

McCown, T.D., Keith, A., 1939. The Stone Age of Mt. Carmel II, The Fossil Human Remains from the Levalloiso-Mousterian. Oxford University Press, Oxford.

Meignen, L., Bar-Yosef, O., 2020. Acheulo-Yabrudian and Early Middle Paleolithic at Hayonim Cave (Western Galilee, Israel): Continuity or break? Journal of Human Evolution 139, 102733.

Meignen, L., Bar-Yosef, O., Speth, J.D., Stiner, M.C., 2006. Middle Paleolithic settlement patterns in the Levant. Transitions before the transition: Evolution and stability in the Middle Paleolithic and Middle Stone Age, 149-169.

Mercier, N., Valladas, H., 2003. Reassessment of TL age estimates of burnt flints from the Paleolithic site of Tabun Cave, Israel. Journal of Human Evolution 45, 401-409.

Mercier, N., Valladas, H., Falguères, C., Shao, Q., Gopher, A., Barkai, R., Bahain, J.-J., Vialettes, L., Joron, J.-L., Reyss, J.-L., 2013. New datings of Amudian layers at Qesem

Cave (Israel): results of TL applied to burnt flints and ESR/U-series to teeth. Journal of Archaeological Science 40, 3011-3020.

Mercier, N., Valladas, H., Froget, L., Joron, J.-L., Ronen, A., 2000. Datation par thermoluminescence de la base du gisement paléolithique de Tabun (mont Carmel, Israël). Comptes Rendus de l'Académie des Sciences - Series IIA - Earth and Planetary Science 330, 731-738.

Mercier, N., Valladas, H., Froget, L., Joron, J.L., Reyss, J.L., Weiner, S., Goldberg, P., Meignen, L., Bar-Yosef, O., Belfer-Cohen, A., Chech, M., Kuhn, S.L., Stiner, M.C., Tillier, A.M., Arensburg, B., Vandermeersch, B., 2007. Hayonim Cave: a TL-based chronology for this Levantine Mousterian sequence. Journal of Archaeological Science 34, 1064-1077.

Mercier, N., Valladas, H., Joron, J.L., Schiegl, S., Bar Yosef, O., Weiner, S., 1995a. Thermoluminescence Dating and the Problem of Geochemical Evolution of Sediments - A Case Study: The Mousterian Levels at Hayonim. Israel Journal of Chemistry 35, 137-141.

Mercier, N., Valladas, H., Valladas, G., Reyss, J.L., Jelinek, A., Meignen, L., Joron, J.L., 1995b. TL Dates of Burnt Flints from Jelinek's Excavations at Tabun and their Implications. Journal of Archaeological Science 22, 495-509.

Murray, A.S., Wintle, A.G., 2000. Luminescence dating of quartz using an improved single-aliquot regenerative-dose protocol. Radiation Measurements 32, 57-73.

Oron, M., Hovers, E., Porat, N., Roskin, J., Abulafia, T., 2024. Nubian Levallois Technology During MIS 5: Refitted Lithic Sequences and OSL Ages of Dimona South, Israel, and Their Broader Implications. Journal of Paleolithic Archaeology 7, 4.

Prescott, J.R., Hutton, J.T., 1988. Cosmic ray and gamma ray dosimetry for TL and ESR. International Journal of Radiation Applications and Instrumentation. Part D. Nuclear Tracks and Radiation Measurements 14, 223-227.

Rak, Y., 1998. Does any Mousterian cave present evidence of two hominid species?, in: Akazawa, T., Aoki, K., Bar-Yosef, O., Neandertals and Modern Humans in Western Asia. , N.Y., pp. 353–366. (Eds.), Neandertals and modern humans in western Asia. Plenum Press, New York, pp. 353-366.

Richter, D., Richter, A., Dornich, K., 2015. Lexsyg smart - a luminescence detection system for dosimetry, material research and dating application. Geochronometria 42, 202-209.

Rink, W.J., Schwarcz, H.P., Ronen, A., Tsatskin, A., 2004. Confirmation of a near 400 ka age for the Yabrudian industry at Tabun Cave, Israel. Journal of Archaeological Science 31, 15-20.

Ronen, A., Gisis, I., Tchernikov, I., 2011. The Mugharan tradition reconsidered. The Lower and Middle Paleolithic in the Middle East and neighboring regions 126, 59e66.

Schiegl, S., Lev-Yadun, S., Bar-Yosef, O., El Goresy, A., Weiner, S., 1994. Siliceous aggregates from prehistoric wood ash: a major component of sediments in Kebara and Hayonim caves (Israel). Israel Journal of Earth Sciences 43, 257-278.

Shea, J.J., 2014. Sink the Mousterian? Named stone tool industries (NASTIES) as obstacles to investigating hominin evolutionary relationships in the Later Middle Paleolithic Levant. Quaternary International 350, 169-179.

Shimelmitz, R., Kuhn, S.L., Bisson, M., Weinstein-Evron, M., 2021. The end of the Acheulo-Yabrudian and the Lower Paleolithic in the Levant: a view from the "transitional" Unit X of Tabun Cave, Israel. Archaeological and Anthropological Sciences 13, 66.

Shimelmitz, R., Kuhn, S.L., Jelinek, A.J., Ronen, A., Clark, A.E., Weinstein-Evron, M., 2014. 'Fire at will': The emergence of habitual fire use 350,000 years ago. Journal of Human Evolution 77, 196-203.

Shimelmitz, R., Kuhn, S.L., Weinstein-Evron, M., 2020. The evolution of raw material procurement strategies: A view from the deep sequence of Tabun Cave, Israel. Journal of Human Evolution 143, 102787.

Shimelmitz, R., Weinstein-Evron, M., Ronen, A., Kuhn, S.L., 2016. The Lower to Middle Paleolithic transition and the diversification of Levallois technology in the Southern Levant: Evidence from Tabun Cave, Israel. Quaternary International 409, 23-40.

Thiel, C., Buylaert, J.-P., Murray, A., Terhorst, B., Hofer, I., Tsukamoto, S., Frechen, M., 2011. Luminescence dating of the Stratzing loess profile (Austria) – Testing the potential of an elevated temperature post-IR IRSL protocol. Quaternary International 234, 23-31.

Tillier, A.-M., 2005. The Tabun C1 Skeleton: A Levantine Neanderthal? Mitekufat Haeven: Journal of the Israel Prehistoric Society 35, 439-450.

Valladas, H., Mercier, N., Hershkovitz, I., Zaidner, Y., Tsatskin, A., Yeshurun, R., Vialettes, L., Joron, J.-L., Reyss, J.-L., Weinstein-Evron, M., 2013. Dating the Lower to Middle Paleolithic transition in the Levant: A view from Misliya Cave, Mount Carmel, Israel. Journal of Human Evolution 65, 585-593.

Weiner, S., 2010. Microarchaeology: Beyond the Visible Archaeological Record. Cambridge University Press, Cambridge.

Weiner, S., Goldberg, P., 1990. On-site Fourier transform-infrared spectrometry at an archaeological excavation. Spectroscopy 5, 46-50.

Weiner, S., Goldberg, P., Bar-Yosef, O., 1993. Bone Preservation in Kebara Cave, Israel using On-Site Fourier Transform Infrared Spectrometry. Journal of Archaeological Science 20, 613-627.

Weiner, S., Goldberg, P., Bar-Yosef, O., 2002. Three-dimensional distribution of minerals in the sediments of Hayonim Cave, Israel: diagenetic processes and archaeological implications. Journal of Archaeological Science 29, 1289-1308.

Weissbrod, L., Weinstein-Evron, M., 2022. Early modern human dispersal into southwest Asia occurred in variable climates: a reply to Frumkin and Comay (2019). Journal of Human Evolution 171, 102833.

Wojtczak, D., Malinsky-Buller, A., 2022. The Levantine Early Middle Palaeolithic in retrospect–Reassessing the contribution of Abou-Sif to the understanding of Palaeolithic record. Archaeological Research in Asia 30, 100366.

Zaidner, Y., Centi, L., Prévost, M., Mercier, N., Falguères, C., Guérin, G., Valladas, H., Richard, M., Galy, A., Pécheyran, C., Tombret, O., Pons-Branchu, E., Porat, N., Shahack-Gross, R., Friesem, D.E., Yeshurun, R., Turgeman-Yaffe, Z., Frumkin, A., Herzlinger, G., Ekshtain, R., Shemer, M., Varoner, O., Sarig, R., May, H., Hershkovitz, I., 2021. Middle Pleistocene *Homo* behavior and culture at 140,000 to 120,000 years ago and interactions with *Homo sapiens*. Science 372, 1429-1433.

Zaidner, Y., Weinstein-Evron, M., 2020. The emergence of the Levallois technology in the Levant: A view from the Early Middle Paleolithic site of Misliya Cave, Israel. Journal of Human Evolution 144, 102785.